AMERICAN SOCIETY FOR MICROBIOLOGY | Molecular and Cellular Biology®

RESEARCH ARTICLE

Morphogenesis of the Islets of Langerhans Is Guided by Extraendocrine Slit2 and Slit3 Signals

Jennifer M. Gilbert,[a] Melissa T. Adams,[a] Nadav Sharon,[b] Hariharan Jayaraaman,[a] Barak Blum[a]

[a]Department of Cell and Regenerative Biology, University of Wisconsin—Madison School of Medicine and Public Health, Madison, Wisconsin, USA
[b]Department of Stem Cell and Regenerative Biology, Harvard University, Cambridge, Massachusetts, USA

ABSTRACT The spatial architecture of the islets of Langerhans is vitally important for their correct function, and alterations in islet morphogenesis often result in diabetes mellitus. We have previously reported that Roundabout (Robo) receptors are required for proper islet morphogenesis. As part of the Slit-Robo signaling pathway, Robo receptors function in conjunction with Slit ligands to mediate axon guidance, cell migration, and cell positioning in development. However, the role of Slit ligands in islet morphogenesis has not yet been determined. Here, we report that Slit ligands are expressed in overlapping and distinct patterns in both endocrine and nonendocrine tissues in late pancreas development. We show that the function of either Slit2 or Slit3, which are predominantly expressed in the pancreatic mesenchyme, is required and sufficient for islet morphogenesis, while Slit1, which is predominantly expressed in the β cells, is dispensable for islet morphogenesis. We further show that Slit functions as a repellent signal to β cells. These data suggest that clustering of endocrine cells during islet morphogenesis is guided, at least in part, by repelling Slit2/3 signals from the pancreatic mesenchyme.

KEYWORDS islets of Langerhans, pancreas development, Slit-Robo

Blood glucose homeostasis is regulated in the pancreas by clusters of endocrine cells called the islets of Langerhans. Islets consist of five different endocrine cell types (α, β, δ, PP, and ε), which secrete glucagon, insulin, somatostatin, pancreatic polypeptide, and ghrelin, respectively. Murine islets exhibit a distinct cytoarchitecture consisting of a core of β cells surrounded by a mantle of α, δ, PP, and ε cells. The β-cell core makes up roughly 80% of the islet mass, while the four other cell types make up the remaining 20% (1, 2). Human islet architecture is more complex, but recent work has suggested that even in human islets, homotypic interactions between endocrine cell types are preferred over heterotypic ones (3, 4). Islet cytoarchitecture is thought to be important for proper islet function, and loss of proper architectural makeup is described in obesity and diabetes in both mice and humans (5–8). While the architectural features of islets have been well documented, the mechanisms controlling the formation of this architecture are still largely unknown.

The Slit-Robo signaling pathway has roles in a number of developmental processes, primarily axon guidance, cell movement, and cell adhesion (9–13). Slit ligand binding to Robo receptors can induce cell migration using repulsive or attractive cues in a context-dependent manner. In the developing mouse, Slit-Robo signaling provides a repulsive corridor to prevent migrating axons from straying from their path during innervation (14, 15). Slit-Robo binding inactivates Rho GTPases, inhibiting actin polymerization and driving the cell away from the direction of the Slit signal (11, 13). Conversely, Slit uses attractive cues to promote vascular development and angiogenesis. In this context, Slit-Robo interactions activate Rho GTPases, inducing actin polymerization in the direction of the Slit signal (11, 13, 16, 17). While Slit and Robo are a canonical signaling pair, both components have alternative binding partners; Slit ligands are able to bind

Citation Gilbert JM, Adams MT, Sharon N, Jayaraaman H, Blum B. 2021. Morphogenesis of the islets of Langerhans is guided by extraendocrine Slit2 and Slit3 signals. Mol Cell Biol 41:e00451-20. https://doi.org/10.1128/MCB.00451-20.

Address correspondence to Barak Blum, bblum4@wisc.edu.

Received 26 August 2020
Returned for modification 20 September 2020
Accepted 7 December 2020
Accepted manuscript posted online 14 December 2020
Published 23 February 2021

semaphorins, ephrins, plexin, and neuronatin to regulate cell migration and metabolic function in specific tissues (14, 18–20). Robo receptors can bind the fibronectin leucine-rich transmembrane protein 3 (FLIRT3) and are capable of forming homodimers to induce axonal growth (21–23).

We have recently described a role for Robo receptors in pancreatic islet architecture (24). Specifically, we showed that genetic deletion of *Robo1* and *Robo2* in β cells (*Robo βKO*) results in loss of stereotypic murine islet architecture without affecting β-cell differentiation or maturation. These Robo-depleted islets have a marked invasion of α and δ cells into the β-cell core. Given the conserved role of Slits as the canonical Robo ligands and our recent findings that Robo receptors regulate endocrine cell type sorting in the islet, we set to investigate the role of Slit ligands in islet morphogenesis.

RESULTS

Slit ligands are expressed in different compartments in the developing mouse pancreas. To test the hypothesis that Slits are involved in Robo-mediated control of islet architecture during development, we first examined whether any of the Slit ligands are expressed in the pancreas at the time of islet morphogenesis. We queried a gene expression database, generated by Krentz and colleagues (25), which contains single-cell transcriptome sequencing (scRNA-Seq) data from embryonic mouse pancreata. We found that *Slit1* expression is present in a subset of endocrine progenitor cells at embryonic day 15.5 (E15.5) and becomes enriched in β cells by E18.5. *Slit2* and *Slit3* expression is distributed between pancreatic mesenchyme, acinar, and ductal cell types with negligible expression in the endocrine compartment at both time points (Fig. 1).

To confirm the expression of Slits in the pancreas *in vivo*, we analyzed pancreata from $Slit1^{GFP}$, $Slit2^{GFP}$, and $Slit3^{LacZ}$ mice, which have knock-in reporters at their respective endogenous Slit loci (26, 27). We identified strong GFP expression in $Slit1^{GFP/+}$ mice both in E18.5 and adult islets. This staining pattern overlapped that of insulin, indicating that *Slit1* is expressed in β cells at both stages (Fig. 2A). We did not detect $Slit2^{GFP}$ (Fig. 2A) or $Slit3^{LacZ}$ (Fig. 2B) in either the embryonic or the adult islets. However, $Slit3^{LacZ}$ expression was detected in pancreatic tissues outside the islet at E18.5 (Fig. 2B). $Slit2^{GFP}$ expression was seen in other tissues, indicating that the lack of $Slit2^{GFP}$ signal in the developing pancreas is not caused by a problem with the reporter (Fig. 2C). A previous report by Escot and colleagues identified *Slit3* expression in the developing pancreatic mesenchyme (28). While we were not able to detect pancreatic $Slit2^{GFP}$ expression, data from scRNA-Seq indicate that it is also expressed in pancreatic mesenchyme during development (25). We concluded that *Slit1* is the predominant Slit ligand expressed inside the islets and that *Slit3* and perhaps *Slit2* are expressed outside the islet during pancreatic development.

Loss of a single Slit ligand does not compromise islet architecture. Slit and Robo are conserved binding partners, and loss of Robo in the islets of *Robo βKO* mice results in severely altered islet architecture (24). We hypothesized that if Slits mediate Robo-regulated islet architecture, then eliminating Slit expression would phenocopy the islet organization defects in *Robo βKO* islets. Whole-body *Slit1*-null ($Slit1^{GFP/GFP}$) and *Slit3*-null ($Slit3^{LacZ/LacZ}$) mice are viable to adulthood. We performed positional cell counting on the islets of these mice as previously described (24) to determine whether these mutants exhibited islet organizational defects. In contrast to the phenotype seen in *Robo βKO* islets, individual *Slit1* or *Slit3* mutant islets display completely normal architecture (Fig. 3A and B). α, β, and δ cells remain restricted to their respective niches; the β cells reside in the core, while the α and δ cells remain in the islet mantle. We also found no significant difference between control islets and *Slit1* or *Slit3* mutant islets in islet size (Fig. 3C), circularity (Fig. 3D), endocrine cell number, or endocrine cell ratios (Fig. 3E and F). We assayed glucose metabolism in these mice via intraperitoneal glucose tolerance test (IPGTT). Neither *Slit1* nor *Slit3* mutant animals displayed evidence of impaired glucose tolerance (Fig. 3G). Whole-body *Slit2*-null ($Slit2^{GFP/GFP}$) animals die shortly after birth, so we examined $Slit2^{GFP/GFP}$ animals at E18.5. Evidence of altered

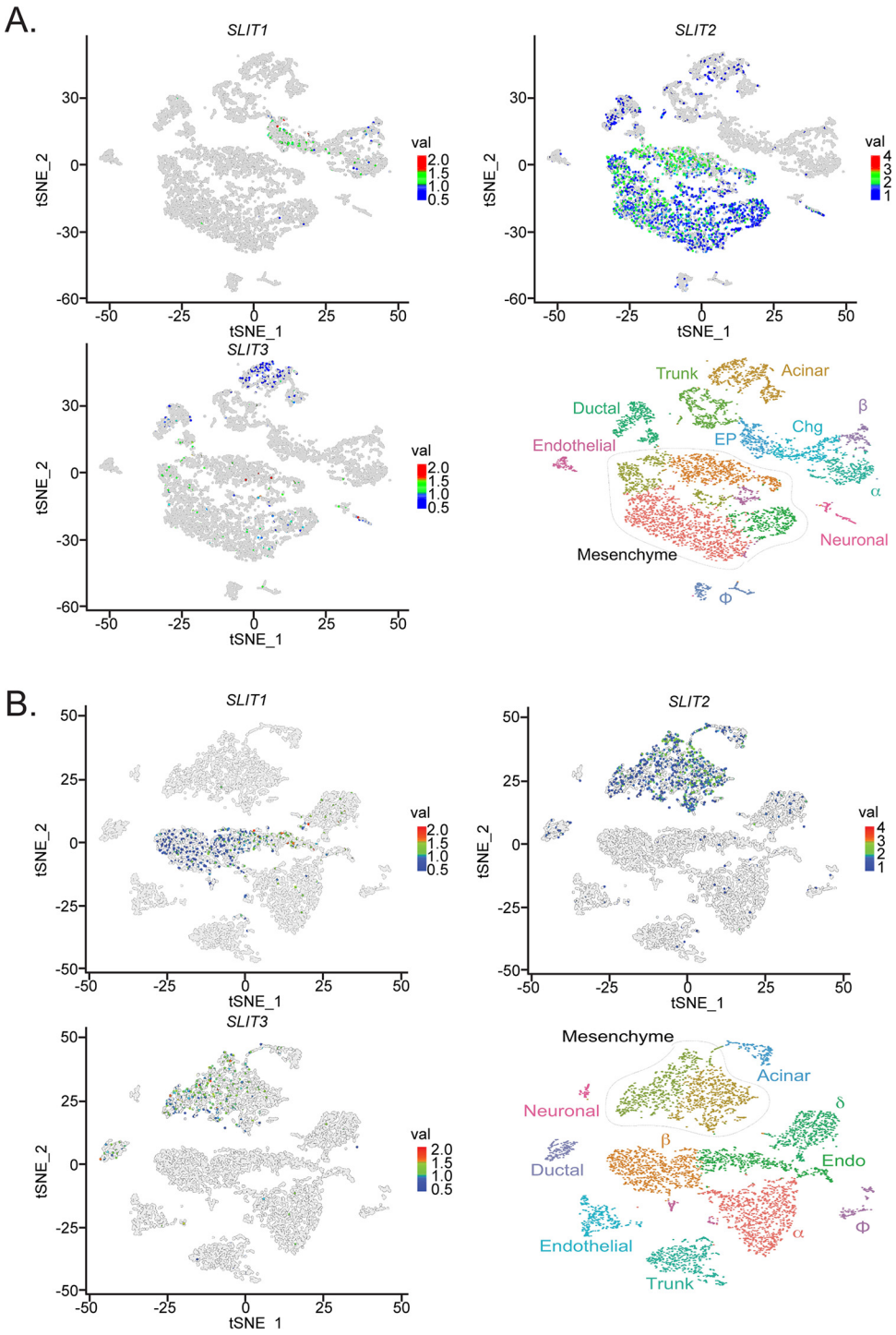

FIG 1 Slit transcripts are expressed in different compartments in the developing murine pancreas. Single-cell RNA-Seq data (scRNA-Seq) were generated using the public database published in Krentz et al. (25). tSNE plots depicting Slit1, Slit2, and Slit3 expression in pancreatic cells. Time points analyzed are E15.5 (A) and E18.5 (B). Slit1 is restricted to the endocrine compartment, while Slit2 and Slit3 localize with the mesenchyme/acinar compartment.

islet architecture in *Robo βKO* mutants can be seen at E18.5; however, we did not observe overt defects in the architecture of *Slit2*$^{GFP/GFP}$ islets at this time point (Fig. 4).

Slit1 is the only Slit we found to be expressed in β cells. Previous work has demonstrated that siRNA-mediated knockdown of Slits in dispersed mouse islet cells induces

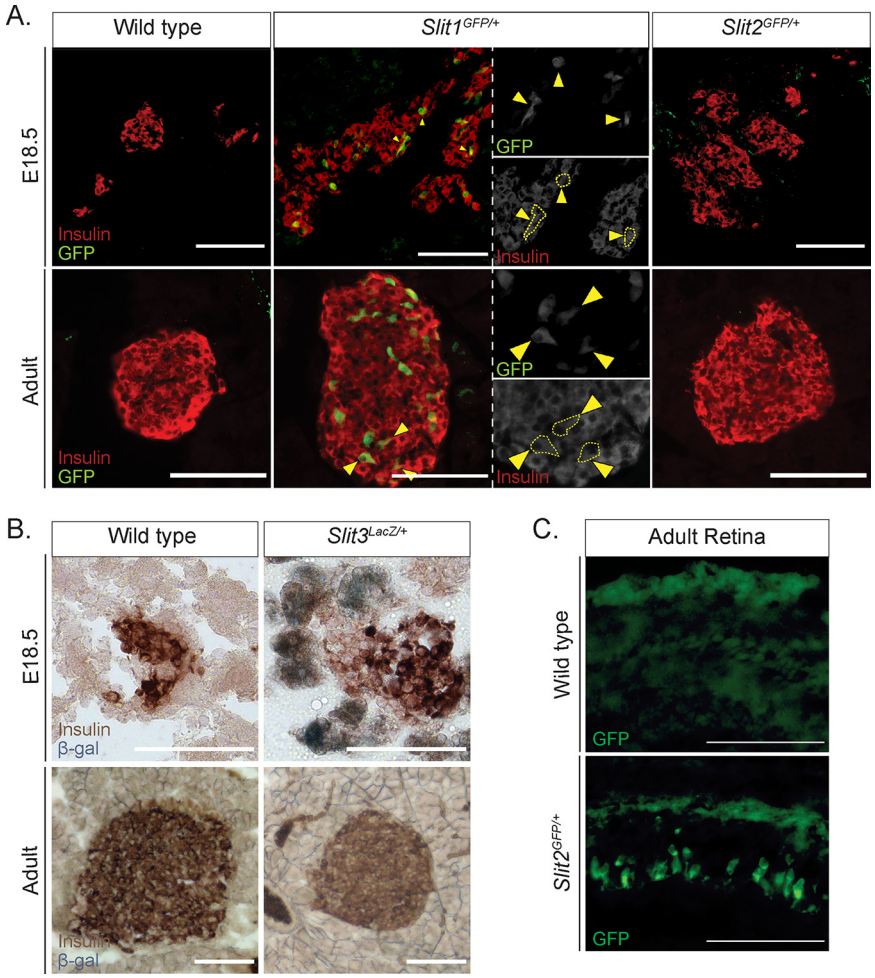

FIG 2 Slit1, but not Slit2 or Slit3, is expressed in the mouse islet from embryonic stages to adulthood. (A) Immunofluorescence staining of β cells (insulin, red) and Slit1 and Slit2 (GFP, green) in E18.5 and adult heterozygous knock-in mice. Arrowheads indicate regions of overlapping GFP and insulin staining, representing Slit1-positive β cells. (B) β-Gal staining of Slit3 (LacZ, blue) in E18.5 and adult heterozygous knock-in mice. β-Gal staining (Slit3 expression) is apparent in nonendocrine tissue surrounding the islet in the embryo. Scale bar, 100 μm. (C) Immunofluorescence staining of Slit2 (GFP, green) in retinal sections from wild-type or Slit2$^{GFP/+}$ heterozygous animals. Scale bars, 100 μm. $n = 3$ for all genotypes at each age analyzed.

apoptosis and that addition of Slits to islets in culture protects β cells from apoptosis and ER stress (29). As the singular Slit ligand expressed in β cells, we tested whether Slit1 conferred a similar protective effect on β cells *in vivo*. To this end, we performed terminal deoxynucleotidyltransferase-mediated dUTP-biotin nick end labeling (TUNEL) analysis on pancreatic sections from lean *Slit1*$^{GFP/GFP}$ animals and wild-type controls as well as on pancreata from obese *Lep*$^{ob/ob}$ and *Lep*$^{ob/ob}$*; Slit1*$^{GFP/GFP}$ animals (Fig. 5). We did not detect an increase in TUNEL-positive nuclei in the β cells from either of the *Slit1*$^{GFP/GFP}$ models, suggesting that loss of Slit1 alone does not induce apoptosis in β cells *in vivo*.

Taken together, these results indicate that individual Slits either are not required for or compensate for each other in the Robo-mediated control of islet architecture.

Slit2 and Slit3 compensate for each other and are required for islet morphogenesis. Slit ligands are highly similar in amino acid sequence, particularly in their Robo-binding domains (30). Thus, it is possible that the different Slit ligands compensate for each other during islet morphogenesis. We tested the extent to which multiple Slit ligands are required for islet architecture by analyzing islet formation in combinatorial Slit mutants. *Slit1*$^{GFP/GFP}$*; Slit3*$^{LacZ/LacZ}$ double knockouts live to adulthood and appear normal, with no detectable alterations in islet architecture, size, circularity,

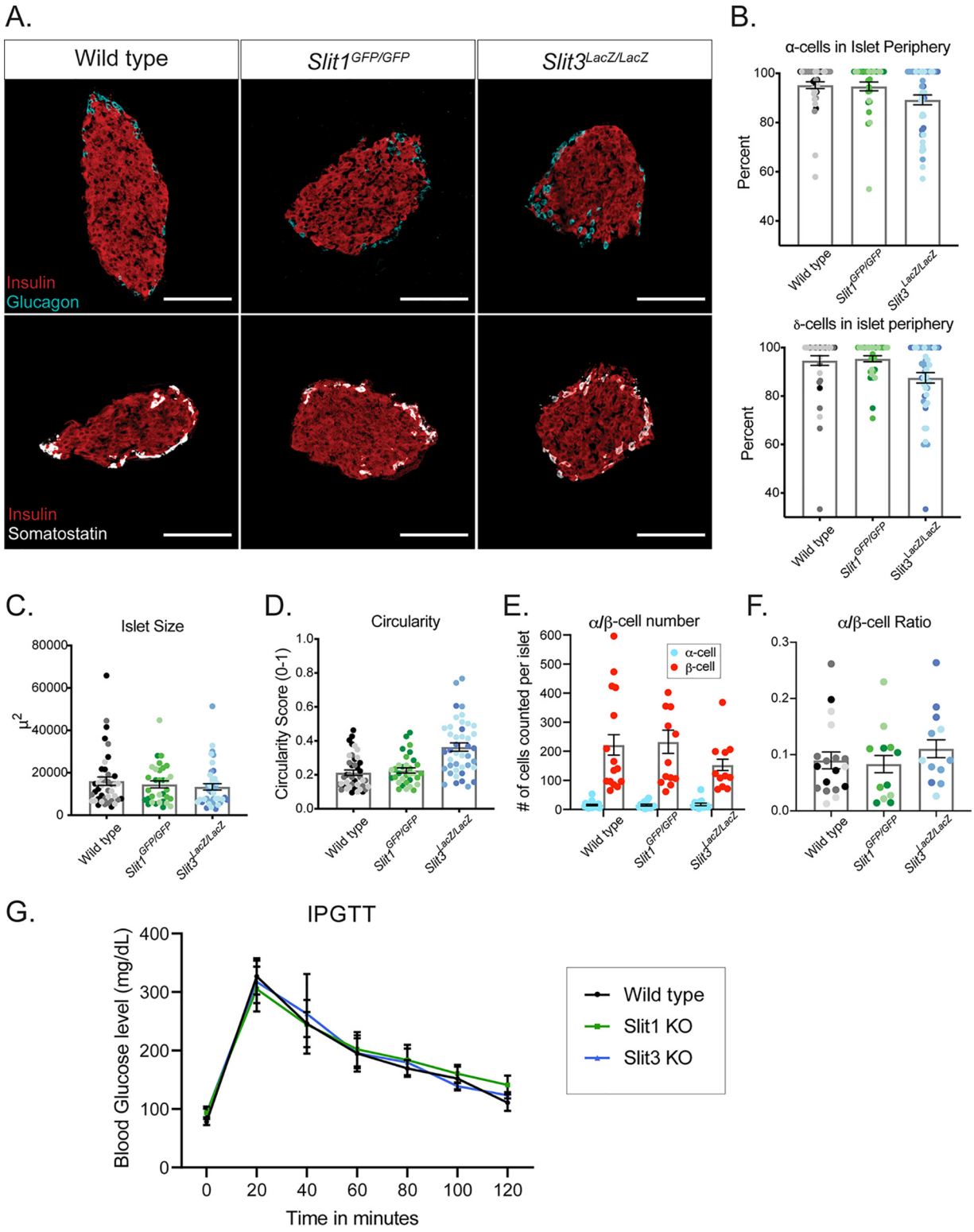

FIG 3 Loss of a single Slit ligand does not compromise islet architecture or glucose metabolism. (A) Immunofluorescence staining of β cells (insulin, red), α cells (glucagon, cyan), and δ cells (somatostatin, white) in adult (~8-week-old) homozygous knockout mice. Scale bars, 100 μm. $n = 3$ for each genotype analyzed. (B) Percentage of α cells and δ cells found in the islet periphery. (C) Average islet size. (D) Average islet circularity (as noted by a circularity score of 0 to 1, where 1 is a perfect circle). (E) α/β-Cell number per islet. (F) α/β-Cell ratio per islet. (G) IPGTT on mice fasted overnight. Wild type, $n = 6$; *Slit1*$^{GFP/GFP}$ (Slit1 KO), $n = 8$; *Slit3*$^{LacZ/LacZ}$ (Slit3 KO), $n = 3$.

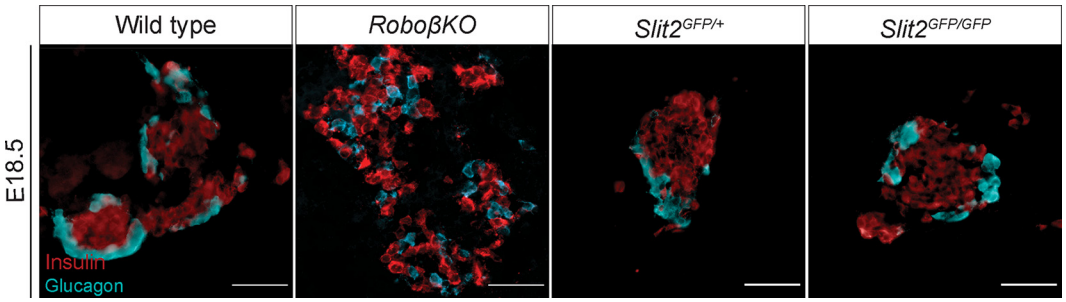

FIG 4 Loss of Slit2 alone does not alter islet architecture. Immunofluorescence staining of β cells (insulin, red) and α cells (glucagon, cyan) in E18.5 control, *Ins2-Cre; Robo1*$^{-/-}$*; Robo2*$^{flx/flx}$, and Slit2 mice. Scale bars, 50 μm. $n = 3$ for all genotypes analyzed.

endocrine cell number, or ratios (Fig. 6A to F). To circumvent the neonatal lethality of *Slit2*$^{GFP/GFP}$ mice, we analyzed the pancreata of *Slit1/2* knockouts (*Slit1*$^{GFP/GFP}$*; Slit2*$^{GFP/GFP}$), *Slit2/3* knockouts (*Slit2*$^{GFP/GFP}$*; Slit3*$^{LacZ/LacZ}$), and *Slit1/2/3* knockouts (*Slit1*$^{GFP/GFP}$*; Slit2*$^{GFP/GFP}$*; Slit3*$^{LacZ/LacZ}$) at E18.5 or at birth (P0). *Slit1/2* knockout islets show no indications of altered architecture, but *Slit2/3* and *Slit1/2/3* knockouts show severely disorganized islets (Fig. 6G). To quantify this phenotype, we scored islets as either intact (insulin-positive cells surrounded by glucagon-positive cells), intermediate (clusters of insulin-positive cells disrupted by glucagon-positive or nonendocrine cells), or disrupted (single cells or clusters of endocrine cells that are not forming islet structures) (Fig. 6H). Double-blinded scoring of islets from the above genotypes revealed that the wild type and *Slit1/2* knockouts have few disrupted islets and similar percentages of intact and intermediate islets (wild type, intact, 49%; intermediate, 40%; disrupted, 11%; *Slit1/2 KO*, intact, 43%; intermediate, 46%; disrupted, 11%). On the other hand, *Slit2/3* and *Slit1/2/3* knockouts had very few intact islets and increased numbers of intermediate and disrupted islets (*Slit2/3 KO*, intact, 8%; intermediate, 53%; disrupted, 39%; *Slit1/2/3 KO*, intact, 8%; intermediate, 60%; disrupted, 32%). Interestingly, we observed a slight reduction in endocrine cell number in *Slit1/2* knockouts and a reduction in β-cell number in *Slit2/3* knockouts but not in the complete triple knockout (Fig. 6I and J). Taken together, the data suggest that *Slit1* (expressed in the islet itself) is dispensable, while *Slit2* and *Slit3* (expressed outside the islet) compensate for each other and are required for proper islet formation.

Slits act as repellent factors to influence β-cell migration. Because *Slit2/3* and *Slit1/2/3* mutant islets are disrupted and do not cluster tightly, we wondered whether this indicates failure of β cells to migrate properly during islet morphogenesis. To test this hypothesis, we performed Transwell cell migration assays using INS-1 cells. INS-1 cells seeded in the top chamber of a cell culture insert above INS-1 conditioned media showed strong migratory activity, while INS-1 cells seeded above fresh, untreated INS-

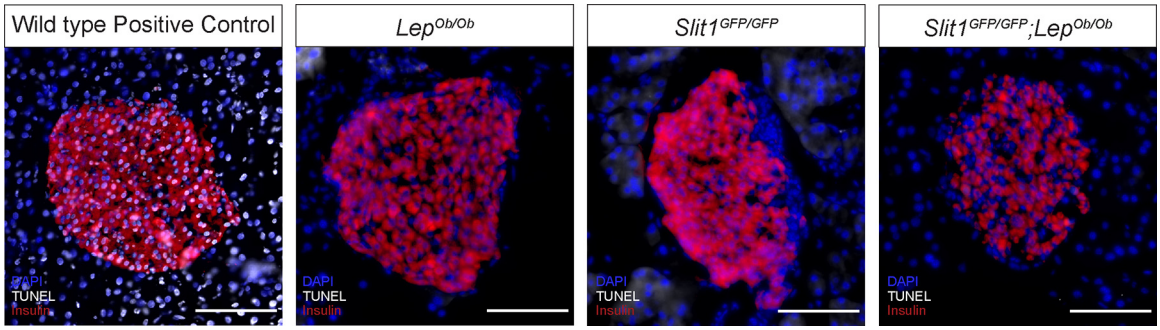

FIG 5 Loss of Slit1 does not increase apoptosis in β cells *in vivo*. Pancreatic sections belonging to *Lep*$^{Ob/Ob}$, *Slit1*$^{GFP/GFP}$, and *Lep*$^{Ob/Ob}$*; Slit1*$^{GFP/GFP}$ animals were assayed for apoptosis using TUNEL (gray) and counterstained for insulin to identify islets. The positive control is a wild-type islet incubated with DNase I. Scale bars, 100 μm. $n = 3$ for all genotypes analyzed.

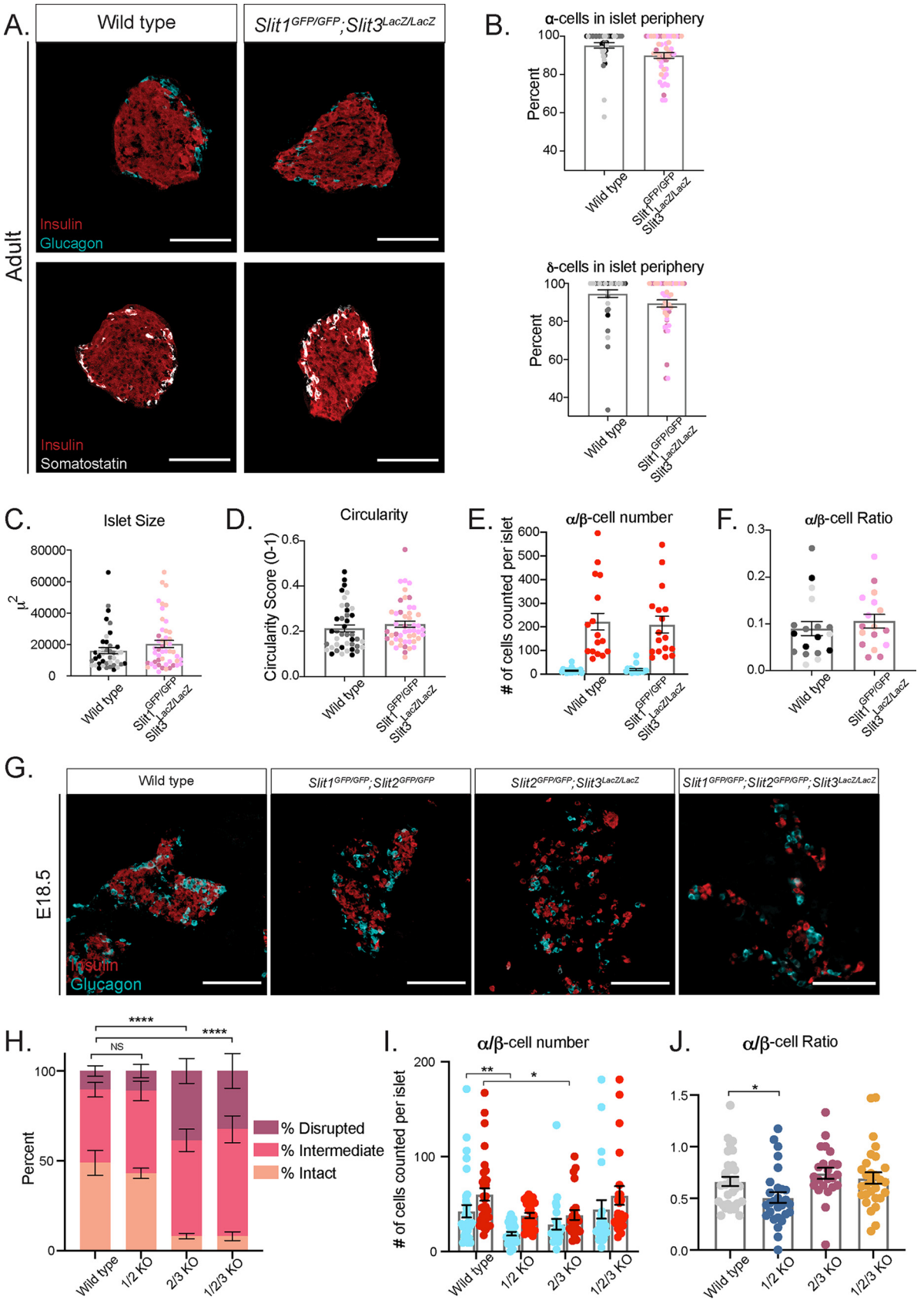

FIG 6 Slit2 and Slit3 compensate for one another in islet morphogenesis. (A) Immunofluorescence staining of β cells (insulin, red), α cells (glucagon, cyan), and δ cells (somatostatin, white) in adult (~8-week-old) homozygous *Slit1*$^{GFP/GFP}$; *Slit3*$^{LacZ/LacZ}$ knockout mice.

(Continued on next page)

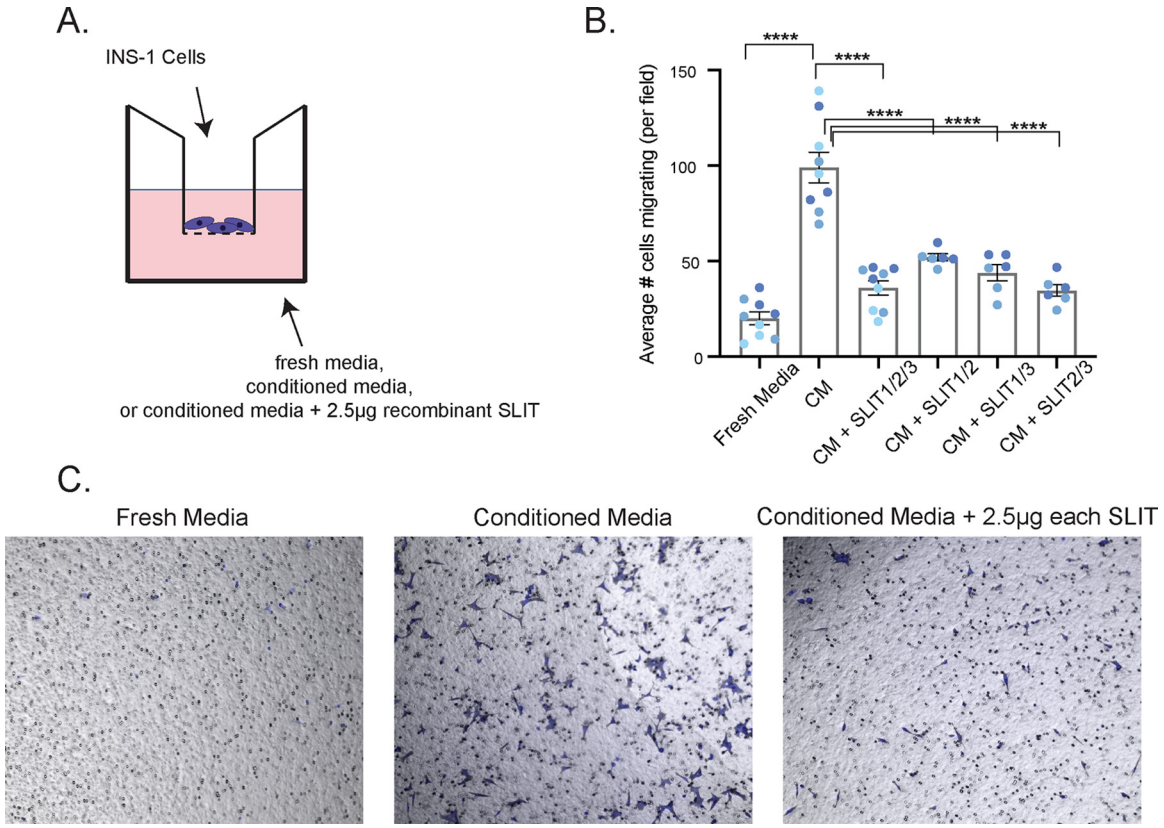

FIG 7 Slits act as repellent factors to influence β-cell migration. (A) Schematic diagram of Transwell cell migration assay. INS-1 cells were seeded in cell culture inserts over INS-1 conditioned media, fresh culture media ($n = 9$), or INS-1 conditioned media supplemented with 2.5 μg of each recombinant SLIT protein ($n = 6$). (B) Results of cell migration assay. The average number of cells migrating per field of view is plotted. ****, $P < 0.0001$ by ANOVA with Tukey-Kramer *post hoc* tests. (C) Representative images of a single field of view of a cell migration insert used in the experiments shown in panel B.

1 culture media did not (Fig. 7). INS-1 cells seeded above conditioned media supplemented with 2.5 μg recombinant SLIT1, SLIT2, and SLIT3 displayed a significantly reduced ability to migrate (Fig. 7B and C), suggesting that Slits influence β-cell migration through cell-cell repulsion mechanisms during islet morphogenesis.

DISCUSSION

In this study, we demonstrate that Slit ligands are required for pancreatic islet architecture. The simultaneous loss of all three Slits results in a disrupted, highly fragmented islet phenotype, which is also observed in *Slit2*$^{GFP/GFP}$; *Slit3*$^{LacZ/LacZ}$ knockouts. These findings lead us to conclude that Slit1 is dispensable for, and that *Slit2* and *Slit3* are required for and have redundant roles in, islet morphogenesis. While our analysis was conducted largely in two dimensions (2D), recent work by the Hara group suggests that 3D analysis of our islets and the encompassing microenvironment will reveal more detailed patterns of our phenotype (31).

The exact mechanism of Slits in islet morphogenesis is unknown; however, the expression pattern of Robo in the pancreas provides some clues. Slit and Robo are

FIG 6 Legend (Continued)
Scale bars, 100 μm. (B) Percentage of α cells and δ cells found in the islet periphery. (C) Average islet size. (D) Average islet circularity (as noted by a circularity score of 0 to 1, where 1 is a perfect circle). (E) α/β-Cell number per islet. (F) α/β-Cell ratio per islet. (G) Immunofluorescence staining of β cells (insulin, red) and α cells (glucagon, cyan) in wild-type, double, and triple knockout mice at E18.5/P0. Scale bars, 100 μm. (H) Percentages of islets from each genotype that were scored as intact, intermediate, or disrupted. ****, $P < 0.0001$ by chi-square test. (I) α/β-Cell number per islet. *, $P < 0.05$; **, $P < 0.01$. (J) α/β-Cell ratio per islet. *, $P < 0.05$. $n = 3$ for all genotypes at each age analyzed.

ligand-receptor binding partners in their eponymous signaling pathway. During mammalian development, Slit and Robo occupy adjacent tissues, specifying complementary expression patterns in the developing organism (30). While all three Slits have expression patterns unique to their specific domain, they also have overlapping regions of expression, suggesting some genetic redundancy. Interestingly, *Slit2* and *Slit3* share more expression domains with each other than either of them do with *Slit1* (30). We have observed a similar framework in the mouse pancreas during islet morphogenesis: *Robo* is primarily expressed in endocrine cells (24), while *Slit2* and *Slit3* have overlapping expression patterns in extraendocrine tissue. While we were not able to detect the $Slit2^{GFP}$ reporter in the pancreas (perhaps due to low expression levels or timing of expression), alternative detection methods, such as *in situ* hybridization, may more definitively pinpoint *Slit2* localization in the pancreas.

Complementary and overlapping regions of expression are hallmarks of ligand-receptor binding partners and suggest that extraendocrine Slit2 and Slit3 interact with endocrine Robo to coordinate islet morphogenesis. We propose that Slit2/3 signals are picked up by Robo receptors on the surface of developing islet endocrine cells. These endocrine cells are then repelled from the direction of the Slit signal, allowing for islet clustering to occur. Loss of this signal results in a failure of islet morphogenesis and, thus, the fragmented phenotype described above. It is likely that Slits are not the only signal required for morphogenesis, as a small number of islets in $Slit2^{GFP/GFP}$; $Slit3^{LacZ/LacZ}$ and triple knockout animals still showed evidence of appropriate clustering. Future work will determine whether other ligands or even Robo-Robo interactions are involved in islet morphogenesis.

It is commonly held that islet morphogenesis is outlined by delamination of endocrine progenitors from the pancreatic duct, followed by their migration as individual cells through the mesenchyme and aggregation into islets (32), implying that β cells respond to attractive cues from the islets. Indeed, we have observed strong Transwell migration of β cells toward their own conditioned medium, demonstrating that β cells are attracted to β cells. However, we further provide evidence to suggest mesenchymal Slits repel β cells during islet morphogenesis. These results are in support of the recent observation that endocrine progenitors remain physically connected throughout islet morphogenesis (33) and suggest that after β-cell delamination, repulsion of the β cells by mesenchymal Slits pushes them into the center of the islet, thereby maintaining the core-mantle architecture. Taking these results together, we propose that both attractive and repulsive signals operate together in forming the canonical murine islet architecture. Of note is that the experiments performed here were done on islets at relatively late stages of development (E18.5 to adult). Given the expression and function of both Robo and Slit in the early pancreas (28, 34), it is plausible that Slit and Robo affect not only islet clustering but also earlier stages of islet development. Further work will hopefully test the role of Slit and Robo in endocrine cell delamination.

The role of *Slit1* in islet morphogenesis remains elusive. The islet architecture phenotypes seen in $Slit2^{GFP/GFP}$; $Slit3^{LacZ/LacZ}$ animals are not significantly different in triple knockouts, suggesting that *Slit1* does not have any influence on islet architecture. In addition, *Slit1* expression does not overlap that of *Slit2* or *Slit3*, so it is unlikely to be redundant. Thus, it is plausible that *Slit1* is tasked with other roles in the islet while the transient expression of *Slit2* and *Slit3* in the mesenchyme during development is responsible for islet morphogenesis. How the expression of *Slit1* in β cells does not interfere with the function of Slit2 and Slit3 from the mesenchyme during islet morphogenesis is intriguing and remains to be elucidated.

Islet structure is closely linked to islet function. The generation of islets from human iPS cells for transplantation into diabetic patients is a promising therapeutic. However, current research efforts have not been able to completely recapitulate the full gene expression or three-dimensional organization of human islets *in vitro*. Thus, elucidating the roles of Slit and Robo in islet organization may be beneficial to the development of bona fide islets from stem cells *in vitro*.

MATERIALS AND METHODS

Animals. All animal experiments were conducted in accordance with the University of Wisconsin—Madison IACUC guidelines under approved protocol number M005221. *Robo1*$^{-}$; *Robo2*^{flx} (35), *Ins2-Cre* (36), *H2B-mCherry* (37), *Slit1*^{GFP}; *Slit2*^{GFP} (26), *Slit3*^{LacZ} (27), and *Lep*^{ob} (38) alleles have been previously described.

Expression analysis. *t*-distributed stochastic neighbor embedding (tSNE) plots of scRNA-Seq were obtained from the Lynn Lab's Single-Cell Gene Expression Atlas (https://lynnlab.shinyapps.io/embryonic_pancreas/) (25).

Immunostaining. Pancreata were dissected from adult (~8-week-old), embryonic (E18.5), or newborn (P0) mice, fixed in 4% paraformaldehyde for 1 h at room temperature (20 to 30 min for E18.5 and P0), preserved in 30% sucrose, embedded in OCT (Leica), and sectioned onto slides. Slides were stained according to the following protocol: 1-h block in 10% normal donkey serum in phosphate-buffered saline with Tween 20 (PBST), 1-h primary antibody incubation, three 10-min PBST washes, 1-h secondary antibody incubation in the dark, three 10-min PBST washes, and mounting of slides in Fluoromount-G (Thermo Fisher). The following primary antibodies were used: guinea pig anti-insulin, 1:800 (Dako), guinea pig anti-insulin, prediluted 1:6 (Dako, 1R002), chicken anti-green fluorescent protein (anti-GFP), 1:1,000 (ab13970; Abcam), rabbit antiglucagon, 1:200 (2760; Cell Signaling), goat antisomatostatin, 1:50 (Santa Cruz), rabbit antisomatostatin, 1:800 (G-060-03; Phoenix), and 4′,6-diamidino-2-phenylindole (DAPI), 1:10,000 (9542; Sigma). The following secondary antibodies were used at 1:500: Alexa Fluor 647–anti-guinea pig antibody, Alexa Fluor 594–anti-rabbit antibody, Alexa Fluor 594–anti-goat antibody, Alexa Fluor 488–anti-rabbit antibody, and Alexa Fluor 488–anti-chicken antibody.

For TUNEL analysis, $n = 3$ animals of each genotype were analyzed. Tissue sections were microwaved at 300 W for 3 min in 0.1 M citrate buffer. Slides were washed in 1× PBS and then blocked and incubated with primary antibodies as detailed above. Positive-control slides were incubated with DNase I (1,000 Kunitz units/ml in Tris-HCl with 1% bovine serum albumin [BSA]) for 5 min and then rinsed with 1× PBST. Slides were incubated with TUNEL staining solution (Roche) for 1 h at 37°C. Slides were washed in 1× PBST and incubated with secondary antibodies as detailed above.

For eye analysis, $n = 3$ animals of each genotype were analyzed. Tissues were dissected and fixed in 4% paraformaldehyde for 2 h at 4°C. Tissues were preserved in a series of sucrose solutions (10% and 20% sucrose) for 1.5 h each. Tissues were further preserved in 30% sucrose overnight, embedded in OCT, and then sectioned and stained as described above.

For β-galactosidase (β-gal) staining, $n = 3$ animals of each genotype were analyzed. Tissues were fixed in 4% paraformaldehyde for 1 h at room temperature (or 20 to 30 min for E18.5 tissue). Fixed tissues were stained with 5-bromo-4-chloro-3-indolyl-β-D-galactopyranoside (X-Gal) solution (11828673001; Roche) for 22 h at 37°C and then preserved, embedded, and sectioned as described above. Insulin staining on these tissues was done using the Vectastain ABC horseradish peroxidase kit (PK-4007; Vector Labs) and NovaRED kit (SK-4800; Vector Labs) and mounted with VectaMount (H-5000; Vector Labs). Slides for expression analysis were imaged using a Zeiss Axio Observer Z1.

Cell counting and shape and size analysis. Slides used for cell counting or shape and size analysis were imaged on a Nikon A1RS confocal microscope. Confocal z-stacks were converted to maximum intensity projected images. α, β, and δ cells were counted using the ImageJ Cell Counter tool. α or δ cells were considered in the islet periphery if they were within the first two cell layers of the islet. For shape and size analysis, islets were outlined and a threshold was applied in ImageJ. The Analyze Particles tool then gave readout of islet size in square micrometers and a circularity score (between 0 and 1, where 1 indicates a perfect circle). A minimum of 10 islets were analyzed across at least three different tissue sections per mouse. Analyses were performed on $n = 3$ mice for each genotype. α- and δ-cell percentages, islet size, and islet circularity values were averaged for each mouse and plotted in Prism.

Islet scoring. Islet scoring was performed on images of tissue sections stained for insulin, glucagon, and DAPI. z-stack images were converted to maximum intensity projected images and randomly assigned a number identifier. Four independent trials (by four different researchers) of double-blinded scoring were performed on 197 images, comprising at least 10 images spanning four different tissue sections per mouse, $n = 3$ mice per genotype.

IPGTT. Mice were fasted overnight, and initial blood glucose measurements were recorded before intraperitoneal injection of each mouse with 20% glucose in 1× PBS at 2 g/kg mouse body weight. Mice were injected at 30-s intervals, and blood glucose measurements were recorded every 20 min for the following 2 h.

Transwell cell migration assay. INS-1 cells (AddexBio) were maintained in culture medium containing RPMI 1640 (ThermoFisher), 10% fetal bovine serum, and 1% penicillin-streptomycin and supplemented with 0.05 mM β-mercaptoethanol. Cells were seeded at a density of 250,000 cells/ml in Transwell cell culture inserts with 8-μm pores (Sigma). Inserts were placed into wells containing either 700 μl culture medium, 700 μl INS-1 conditioned medium, or 700 μl INS-1 conditioned medium supplemented with 2.5 μg each recombinant SLIT1, SLIT2, and SLIT3 (R&D Systems) and cultured at 37°C for 48 h. Inserts were then fixed in 4% paraformaldehyde for 20 min, unmigrated cells were wiped off the top of the insert, inserts were incubated in 0.08% crystal violet, and a 1:1,000 concentration of DAPI was used to visualize the cells. Nine nonoverlapping field-of-view images were taken for each insert. Three images per insert were chosen at random for quantification. Results are reported as the average number of cells that migrated per field of view.

Statistical analysis. All data are reported as means ± standard errors of the means unless otherwise indicated. *P* values were calculated using Student's *t* test or analysis of variance (ANOVA) with Tukey-

Kramer *post hoc* tests in Prism GraphPad 7 unless otherwise indicated. Any P value of <0.05 was considered significant and marked with an asterisk.

ACKNOWLEDGMENTS

We thank members of the Blum laboratory, especially Bayley Waters and Dex Nimkulrat, for technical help and valuable discussion and comments on the manuscript. We thank Le Ma, David Ornitz, Alain Chedotal, and Marc Tessier-Lavigne for mice. We are grateful to Francis Lynn and Nicole Krentz for allowing us to use their scRNA-Seq data and to Cody Frederickson for help generating figures. We are also grateful to Lance Rodenkirch and the UW—Madison Optical Imaging Core for help with imaging.

This work was funded in part by R01DK121706 from the NIDDK, the DRC at Washington University Pilot Grant P30DK020579, and Pilot Award UL1TR000427 from the UW—Madison Institute for Clinical and Translational Research (ICTR). J.M.G. and M.T.A. were funded by 5T32GM007133-44, a graduate training award from the UW—Madison Stem Cell & Regenerative Medicine Center, and an Advanced Opportunity Fellowship through SciMed Graduate Research Scholars at UW—Madison.

Conceptualization, B.B. and J.M.G.; Methodology, B.B. and J.M.G.; Investigation, J.M.G., M.T.A., N.S., and H.J.; Formal Analysis, J.M.G., M.T.A., N.S., and H.J.; Writing—Original Draft, B.B. and J.M.G.; Writing, Review, and Editing, all authors; Funding Acquisition, B.B.; Supervision, B.B.

REFERENCES

1. Kim A, Miller K, Jo J, Kilimnik G, Wojcik P, Hara M. 2009. Islet architecture: a comparative study. Islets 1:129–136. https://doi.org/10.4161/isl.1.2.9480.
2. Steiner DJ, Kim A, Miller K, Hara M. 2010. Pancreatic islet plasticity: interspecies comparison of islet architecture and composition. Islets 2:135–145. https://doi.org/10.4161/isl.2.3.11815.
3. Dybala MP, Hara M. 2019. Heterogeneity of the human pancreatic islet. Diabetes 68:1230–1239. https://doi.org/10.2337/db19-0072.
4. Hoang DT, Matsunari H, Nagaya M, Nagashima H, Millis JM, Witkowski P, Periwal V, Hara M, Jo J. 2014. A conserved rule for pancreatic islet organization. PLoS One 9:e110384. https://doi.org/10.1371/journal.pone.0110384.
5. Baetens D, Stefan Y, Ravazzola M, Malaisse-Lagae F, Coleman DL, Orci L. 1978. Alteration of islet cell populations in spontaneously diabetic mice. Diabetes 27:1–7. [340309]. https://doi.org/10.2337/diab.27.1.1.
6. Cabrera O, Berman DM, Kenyon NS, Ricordi C, Berggren PO, Caicedo A. 2006. The unique cytoarchitecture of human pancreatic islets has implications for islet cell function. Proc Natl Acad Sci U S A 103:2334–2339. https://doi.org/10.1073/pnas.0510790103.
7. Kilimnik G, Zhao B, Jo J, Periwal V, Witkowski P, Misawa R, Hara M. 2011. Altered islet composition and disproportionate loss of large islets in patients with type 2 diabetes. PLoS One 6:e27445. https://doi.org/10.1371/journal.pone.0027445.
8. Roscioni SS, Migliorini A, Gegg M, Lickert H. 2016. Impact of islet architecture on beta-cell heterogeneity, plasticity and function. Nat Rev Endocrinol 12:695–709. https://doi.org/10.1038/nrendo.2016.147.
9. Blockus H, Chedotal A. 2016. Slit-Robo signaling. Development 143:3037–3044. https://doi.org/10.1242/dev.132829.
10. Chedotal A. 2007. Slits and their receptors. Adv Exp Med Biol 621:65–80. https://doi.org/10.1007/978-0-387-76715-4_5.
11. Wu MF, Liao CY, Wang LY, Chang JT. 2017. The role of Slit-Robo signaling in the regulation of tissue barriers. Tissue Barriers 5:e1331155. https://doi.org/10.1080/21688370.2017.1331155.
12. Ypsilanti AR, Chedotal A. 2014. Roundabout receptors. Adv Neurobiol 8:133–164. https://doi.org/10.1007/978-1-4614-8090-7_7.
13. Ypsilanti AR, Zagar Y, Chedotal A. 2010. Moving away from the midline: new developments for Slit and Robo. Development 137:1939–1952. https://doi.org/10.1242/dev.044511.
14. Brose K, Bland KS, Wang KH, Arnott D, Henzel W, Goodman CS, Tessier-Lavigne M, Kidd T. 1999. Slit proteins bind Robo receptors and have an evolutionarily conserved role in repulsive axon guidance. Cell 96:795–806. https://doi.org/10.1016/S0092-8674(00)80590-5.
15. Dickson BJ, Gilestro GF. 2006. Regulation of commissural axon pathfinding by slit and its Robo receptors. Annu Rev Cell Dev Biol 22:651–675. https://doi.org/10.1146/annurev.cellbio.21.090704.151234.
16. Rama N, Dubrac A, Mathivet T, Ni Charthaigh RA, Genet G, Cristofaro B, Pibouin-Fragner L, Ma L, Eichmann A, Chedotal A. 2015. Slit2 signaling through Robo1 and Robo2 is required for retinal neovascularization. Nat Med 21:483–491. https://doi.org/10.1038/nm.3849.
17. Zhang B, Dietrich UM, Geng JG, Bicknell R, Esko JD, Wang L. 2009. Repulsive axon guidance molecule Slit3 is a novel angiogenic factor. Blood 114:4300–4309. https://doi.org/10.1182/blood-2008-12-193326.
18. Delloye-Bourgeois C, Jacquier A, Charoy C, Reynaud F, Nawabi H, Thoinet K, Kindbeiter K, Yoshida Y, Zagar Y, Kong Y, Jones YE, Falk J, Chedotal A, Castellani V. 2015. PlexinA1 is a new Slit receptor and mediates axon guidance function of Slit C-terminal fragments. Nat Neurosci 18:36–45. https://doi.org/10.1038/nn.3893.
19. Svensson KJ, Long JZ, Jedrychowski MP, Cohen P, Lo JC, Serag S, Kir S, Shinoda K, Tartaglia JA, Rao RR, Chedotal A, Kajimura S, Gygi SP, Spiegelman BM. 2016. A secreted Slit2 fragment regulates adipose tissue thermogenesis and metabolic function. Cell Metab 23:454–466. https://doi.org/10.1016/j.cmet.2016.01.008.
20. Wright KM, Lyon KA, Leung H, Leahy DJ, Ma L, Ginty DD. 2012. Dystroglycan organizes axon guidance cue localization and axonal pathfinding. Neuron 76:931–944. https://doi.org/10.1016/j.neuron.2012.10.009.
21. Hivert B, Liu Z, Chuang CY, Doherty P, Sundaresan V. 2002. Robo1 and Robo2 are homophilic binding molecules that promote axonal growth. Mol Cell Neurosci 21:534–545. https://doi.org/10.1006/mcne.2002.1193.
22. Leyva-Diaz E, del Toro D, Menal MJ, Cambray S, Susin R, Tessier-Lavigne M, Klein R, Egea J, Lopez-Bendito G. 2014. FLRT3 is a Robo1-interacting protein that determines Netrin-1 attraction in developing axons. Curr Biol 24:494–508. https://doi.org/10.1016/j.cub.2014.01.042.
23. Tong M, Jun T, Nie Y, Hao J, Fan D. 2019. The role of the Slit/Robo signaling pathway. J Cancer 10:2694–2705. https://doi.org/10.7150/jca.31877.
24. Adams MT, Gilbert JM, Hinojosa Paiz J, Bowman FM, Blum B. 2018. Endocrine cell type sorting and mature architecture in the islets of Langerhans require expression of Roundabout receptors in beta cells. Sci Rep 8:10876. https://doi.org/10.1038/s41598-018-29118-x.
25. Krentz NAJ, Lee MYY, Xu EE, Sproul SLJ, Maslova A, Sasaki S, Lynn FC. 2018. Single-cell transcriptome profiling of mouse and hESC-derived pancreatic progenitors. Stem Cell Rep 11:1551–1564. https://doi.org/10.1016/j.stemcr.2018.11.008.
26. Plump AS, Erskine L, Sabatier C, Brose K, Epstein CJ, Goodman CS, Mason CA, Tessier-Lavigne M. 2002. Slit1 and Slit2 cooperate to prevent premature midline crossing of retinal axons in the mouse visual system. Neuron 33:219–232. https://doi.org/10.1016/S0896-6273(01)00586-4.
27. Yuan W, Rao Y, Babiuk RP, Greer JJ, Wu JY, Ornitz DM. 2003. A genetic model for a central (septum transversum) congenital diaphragmatic

hernia in mice lacking Slit3. Proc Natl Acad Sci U S A 100:5217–5222. https://doi.org/10.1073/pnas.0730709100.
28. Escot S, Willnow D, Naumann H, Di Francescantonio S, Spagnoli FM. 2018. Robo signalling controls pancreatic progenitor identity by regulating Tead transcription factors. Nat Commun 9:5082. https://doi.org/10.1038/s41467-018-07474-6.
29. Yang YH, Manning Fox JE, Zhang KL, MacDonald PE, Johnson JD. 2013. Intraislet SLIT-ROBO signaling is required for beta-cell survival and potentiates insulin secretion. Proc Natl Acad Sci U S A 110:16480–16485. https://doi.org/10.1073/pnas.1214312110.
30. Yuan W, Zhou L, Chen JH, Wu JY, Rao Y, Ornitz DM. 1999. The mouse SLIT family: secreted ligands for ROBO expressed in patterns that suggest a role in morphogenesis and axon guidance. Dev Biol 212:290–306. https://doi.org/10.1006/dbio.1999.9371.
31. Dybala MP, Butterfield JK, Hendren-Santiago BK, Hara M. 2020. Pancreatic islets and Gestalt principles. Diabetes 69:1864–1874. https://doi.org/10.2337/db20-0304.
32. Pan FC, Wright C. 2011. Pancreas organogenesis: from bud to plexus to gland. Dev Dyn 240:530–565. https://doi.org/10.1002/dvdy.22584.
33. Sharon N, Chawla R, Mueller J, Vanderhooft J, Whitehorn LJ, Rosenthal B, Gurtler M, Estanboulieh RR, Shvartsman D, Gifford DK, Trapnell C, Melton D. 2019. A peninsular structure coordinates asynchronous differentiation with morphogenesis to generate pancreatic islets. Cell 176:790–804. https://doi.org/10.1016/j.cell.2018.12.003.
34. Cozzitorto C, Mueller L, Ruzittu S, Mah N, Willnow D, Darrigrand JF, Wilson H, Khosravinia D, Mahmoud AA, Risolino M, Selleri L, Spagnoli FM. 2020. A specialized niche in the pancreatic microenvironment promotes endocrine differentiation. Dev Cell 55:150–162. https://doi.org/10.1016/j.devcel.2020.08.003.
35. Branchfield K, Nantie L, Verheyden JM, Sui P, Wienhold MD, Sun X. 2016. Pulmonary neuroendocrine cells function as airway sensors to control lung immune response. Science 351:707–710. https://doi.org/10.1126/science.aad7969.
36. Postic C, Shiota M, Niswender KD, Jetton TL, Chen Y, Moates JM, Shelton KD, Lindner J, Cherrington AD, Magnuson MA. 1999. Dual roles for glucokinase in glucose homeostasis as determined by liver and pancreatic beta cell-specific gene knock-outs using Cre recombinase. J Biol Chem 274:305–315. https://doi.org/10.1074/jbc.274.1.305.
37. Blum B, Roose AN, Barrandon O, Maehr R, Arvanites AC, Davidow LS, Davis JC, Peterson QP, Rubin LL, Melton DA. 2014. Reversal of beta cell de-differentiation by a small molecule inhibitor of the TGFbeta pathway. Elife 3:e02809. https://doi.org/10.7554/eLife.02809.
38. Ingalls AM, Dickie MM, Snell GD. 1950. Obese, a new mutation in the house mouse. J Hered 41:317–318. https://doi.org/10.1093/oxfordjournals.jhered.a106073.